ENHANCEMENT OF COMPOSITE-METAL ADHESION STRENGTH BY MICRO-PATTERNING OF METAL SURFACES

W.S. Kim[1], D.S. Hwang[1], C.J. Jang[2], J.J. Lee[2]*
[1] Satellite structure department, Korea Aerospace Research Institute, Daejeon, Korea
[2] Department of mechanical engineering, KAIST, Daejeon, Korea
* Corresponding author (leejungju@kaist.ac.kr)

Keywords: *adhesive bonding, surface morphology, interfacial toughness, micro-pattern*

1 Introduction

Over the past few decades, polymer-matrix composite materials have replaced metal alloys and developed into the primary candidate for many aerospace structures due to their superior strength-to-weight and stiffness-to-weight ratios [1]. All-composite structure design concept is coming into appearance for future aerospace vehicles. However, at the present time, composites and metals are used together in most aerospace structures, and joining a composite structural member to a metal structural member is inevitable. Adhesive bonding has significant advantages over conventional joining techniques such as riveting, bolting and welding [1-4]. Most of all, adhesively bonded joints can be designed in such a way that every material consisting the joint is used to its full capacity achieving optimized joint performance. This comes from the continuous load transfer between bonded surfaces which gives greater design flexibility than discrete load transfer through mechanical fasteners. In order to obtain optimal structural bonding efficiency (strength-to-weight ratio), interfaces as well as adherends and adhesives are required to be analyzed as objects for optimization. This study attempts to develop a new interface structure modification technique to make strong and reliable composite/metal bonded joints.

It has been reported that the performance of an adhesive boned joint can be improved by changing the nature of the substrate surface chemically or morphologically [5-8]. The purpose of the present work is to demonstrate the effect of micro-morphological modification of metal surfaces on adhesion strength. While former studies have investigated surface morphological changes after employing various surface treatment methods, this study proposes a micro-patterned morphology on metal surfaces as a designed surface topography. Interfacial fracture toughness under various mixed-mode loading condition was measured using SLB (single-leg bending) specimens. The comparison of G_c values between micro-patterned and mechanically abraded interfaces is made. The effect of loading mode on interfacial crack growth is investigated on the basis of crack path observation using microscopic image acquisition technique.

2 Analysis

2.1 Mixed-mode interfacial toughness

In an adhesive joint, a thin adhesive layer can be reasonably regarded as an interface. In this approach, fracture toughness becomes the property of an interface rather than an adhesive material. This is quite true that the adhesion strength depends not only on adhesive materials but also on adherend materials along with surface treatments and bonding processes. Therefore, the facture toughness should be considered as a property of the interface, and the interfacial toughness is influenced by many factors such as adhesives, adherends, surface treatments and bonding processes.

Unlike cracks in homogeneous materials, interface cracks tend to grow under mixed-mode loading conditions along the bi-material interface. Of particular interest, the critical energy release rate (G_c) changes with loading conditions. In other words, interfacial toughness is a function of mode-ratio (G_{II}/G_I). Hence, the crack growth at an interface can be characterized by comparing applied energy release rate with the interfacial toughness at the same mode-ratio [9]:

$$G(\psi) \geq G_C(\psi) \quad \text{where} \quad \psi = \tan^{-1}\sqrt{G_{II}/G_I} \qquad (1)$$

Since the failure criterion (Eq. (1)) can be applied to any adhesively bonded system regardless of joint geometry, interfacial toughness (G_c) is the most excellent representative of adhesion strength.

2.2 Compliance calibration method

A bi-material SLB test, which provides various mixed-mode loading condition [10], was employed to measure the interfacial toughness of a composite/steel bond. Figure 1 shows a schematic diagram of the test. The dimensions of the specimens were miniaturized due to the technical difficulty of micro-patterning on a large area. Micro-patterns were located at the uncracked ligament of 5mm (from the initial crack tip to the loading point).

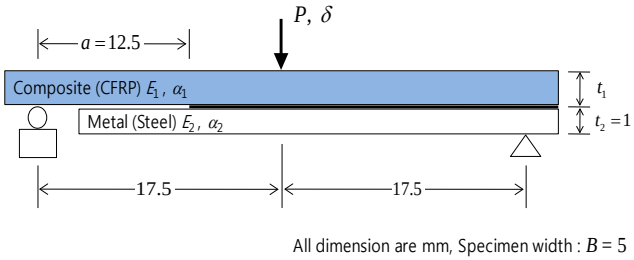

Fig. 1. Schematic representation of the SLB test.

Most standard data reduction schemes to obtain the critical energy release rate (G_c) recommends the compliance calibration method [11-13]. The compliance calibration method is based on the Irwin-Kies equation [14]

$$G_c = \frac{P_c^2}{2B}\frac{dC}{da} \tag{2}$$

where P_c represents the critical (crack on-set) load, B the specimen width and $C = \delta/P$, the compliance. Instead of using beam theory to derive the $C = f(a)$ relationship, experimental determination of the relationship between compliance and crack length enables the consideration of bending and shear effects near the crack tip. The compliance and crack length was normalized as E_1BC and a/t_1 respectively, and the usual form of $C = f(a)$ relationship, $C = k(a+\Delta a)^3$, was reconstructed as :

$$\frac{a}{t_1} = \alpha\left(E_1BC\right)^{1/3} + \beta \tag{3}$$

where α and β are constants that should be determined experimentally. In this way of normalization, $C = f(a)$ relationship can be unified regardless of the upper beam thickness (t_1), which will be varied to control the mode-ratio. Thus, substituting Eq. (3) into Eq. (2), interfacial toughness can be calculated by measuring the crack on-set load (P_c) as :

$$G_c = \frac{3}{2t_1}\left(\frac{P_c}{B}\right)^2\frac{\left(E_1BC\right)^{2/3}}{\alpha E_1} \tag{4}$$

When dissimilar materials are bonded at high temperature, the mismatch of thermal expansion coefficients induces thermal residual stresses. Therefore, residual stress induced energy release rate (G_T) should be included in the total energy release rate as in Eq. (5).

$$G = G_{mech} + G_T + G_{int} \tag{5}$$

where G_{int} is another term resulted from thermal and mechanical load interaction. Nairn [15] calculated the two additional terms in a SLB test specimen based on beam theory and linear elastic fracture mechanics as below.

$$G_T = \frac{1}{2}\frac{E_1t_1\Delta\alpha^2\Delta T^2\left(1+R\lambda^3\right)}{1+R\lambda\left(4+\lambda\left(6+\lambda\left(4+R\lambda\right)\right)\right)} \tag{6}$$

$$G_{int} = \frac{3Pa\Delta T\Delta\alpha\left(R\lambda^2\left(1+\lambda\right)\right)}{Bt_1\left(1+R\lambda\left(4+\lambda\left(6+\lambda\left(4+R\lambda\right)\right)\right)\right)} \tag{7}$$

where $\Delta\alpha=\alpha_1-\alpha_2$, $R=E_1/E_2$, $\lambda=t_1/t_2$. In the present work, interfacial toughness was measured using compliance calibration method, and thermal residual stress effect was also considered using Nairn [15]'s analysis result (Eqs. (6) and (7)).

2.3 Mode decomposition

The total energy release rate, $G=G_I+G_{II}$, was decomposed by decomposing the 3-point bending load applied to the crack tip of a SLB specimen into pure opening and pure sliding mode loadings as shown in Fig. 2.

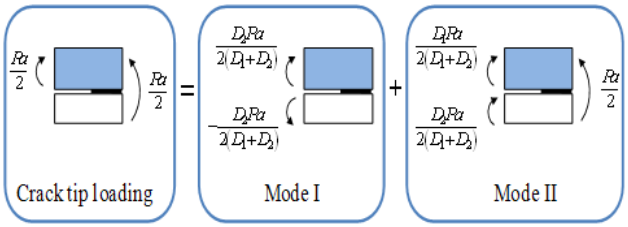

Fig. 2. Loading mode decomposition at the crack tip of a SLB specimen.

The energy release rate at each loading mode can be calculated using beam theory as Eqs. (8) and (9).

$$G_{\mathrm{I}} = \frac{P^2 a^2}{8B}\left(\frac{D_2^2}{(D_1+D_2)^2}\left(\frac{1}{D_1}+\frac{1}{D_2}\right)\right) \tag{8}$$

$$G_{\mathrm{II}} = \frac{P^2 a^2}{8B}\left(\frac{1}{(D_1+D_2)}-\frac{1}{D}\right) \tag{9}$$

where $D_1=E_1I_1$ for upper beam, $D_2=E_2I_2$ for lower beam, and $D=(EI)_{\mathrm{eff}}$ for bonded beam section.

3 Experimental Procedure

3.1 Sample Preparation

Miniaturized composite/steel bonded joints were fabricated. Steel (AISI 1045) plates were cut into 35 × 5 × 1 mm^3 samples and coated with a commercial photoresist (SU-8) and exposed to UV through a transparent mask whose line patterns are spaced by 80μm. After using the conventional photolithography, the steel surfaces not covered by the photoresist films were chemically etched in an etchant called Nital solution (nitric acid and ethanol mixed solution) to fabricate micro-line patterns on the steel surface (Fig. 3). After the surface patterning process, CFRP prepregs (USN-150 from SK Chemical, Korea) were laminated on the steel plate ([0_9/steel]) and bonded through the standard curing process of the CFRP prepreg. In other words, composite and micro-patterned steel were boned using a co-cure bonding method without additional adhesive layer. Micro-patterns were located at the uncracked ligament of 5mm (from the initial crack tip to the loading point). The thickness ratio of SLB specimens was varied as $t_1/t_2 = 0.5,\ 0.75,\ 1.25,\ 2.0$ to produce various mixed-mode loading conditions.

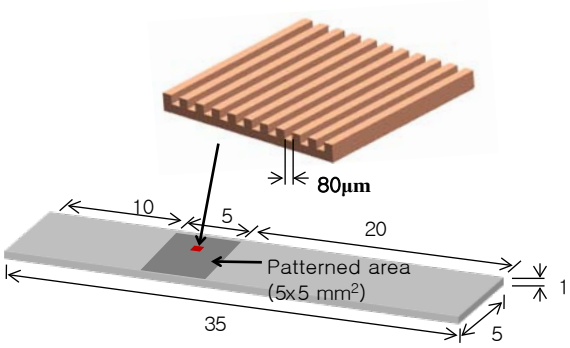

Fig. 3. Schematic representation of a microline-patterned steel specimen.

The lower steel beam thickness was held constant as t_2=1mm, and the upper composite beam thickness (t_1) was controlled by varying the prepreg number laid-up on the steel substrates. An interfacial pre-crack was introduced by smearing mold release agent (NR-650 from Nabakem, Korea) on the steel surface prior to bonding.

3.2 Fracture testing

A miniaturized three-point bend fixture was used as shown in Fig. 4, and the fracture testing was performed under displacement control at a ramp rate of 10μm/sec using a computer-controlled stepper motor. A traveling optical microscope was positioned on one side of the specimen to observe the material behavior near a crack tip during fracture tests. Using CCD camera and computer-based image acquisition equipment, interface images were captured and stored to the computer at a rate of 30 frame/s.

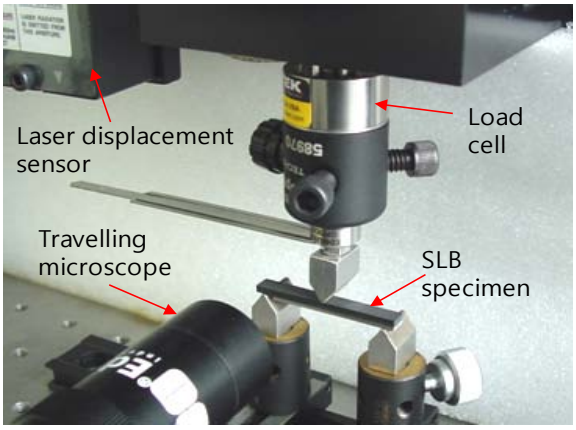

Fig. 4. Miniaturized three-point bending fixture with optical microscope for image acquisition.

4 Results and discussion

4.1 Surface and interface observation

The SEM image in Fig. 5 shows the micro-line patterned steel surface. Micro-scale periodic grooves were fabricated on steel surface. The profiles of the periodic grooves are semicircular due to the isotropic wet-etching process. Optical microscope cross-sectional images in Fig. 6, show the CFRP/steel bonded interface. The line patterned surface provides more roughened surface than the sandpaper abraded surface. The epoxy resin extracted from the CFRP prepreg during the co-cure bonding process successfully filled the micro-grooves on the steel surface. Therefore, mechanical interlocking between the polymer resin and artificially patterned steel surface was completely attained.

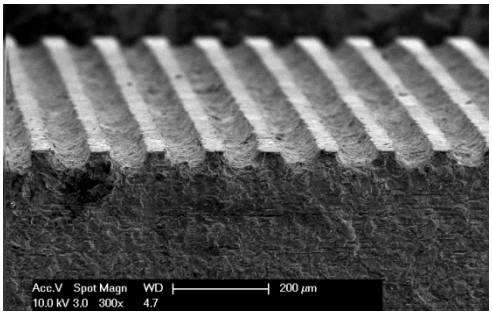

Fig. 5. SEM image of micro-patterned steel surface.

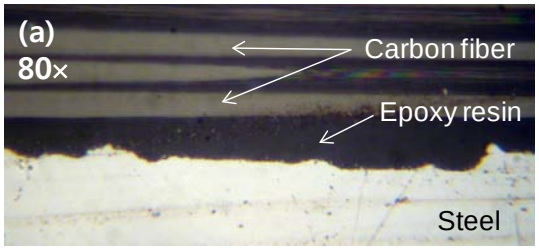

(a) Sandpaper abraded steel surface

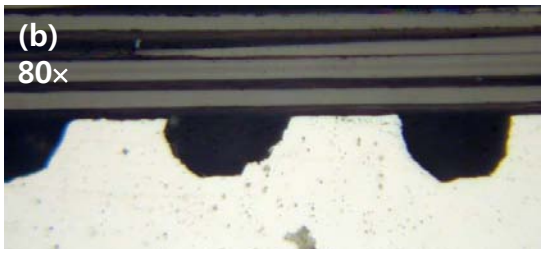

(b) Micro-line patterned steel surface

Fig. 6. Co-cure bonded composite/steel interface

4.2 Adhesion strength of bonded interface

Figure 7 shows the experimental configuration of the 3-point bend test of SLB specimens. Thin composite adherend layer induces crack-opening mode dominant loading while thick composite adherend layer induces crack-sliding mode dominant loading.

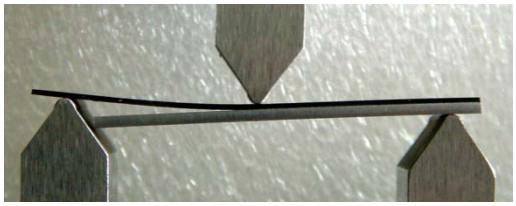

(a) SLB specimen with t_1 = 0.5mm

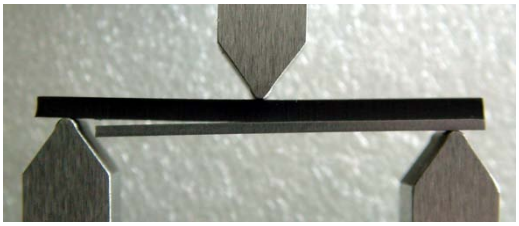

(b) SLB specimen with t_1 = 2mm

Fig. 7. Three-point bend test of SLB specimens.

Typical load-displacement curves from the fracture tests are shown in Fig. 8. The bond strength increases as the crack-sliding mode (mode II) loading component increases. In any mode-ratio, micro-line patterned interface structure achieves higher failure loads than mechanically abraded interface structure.

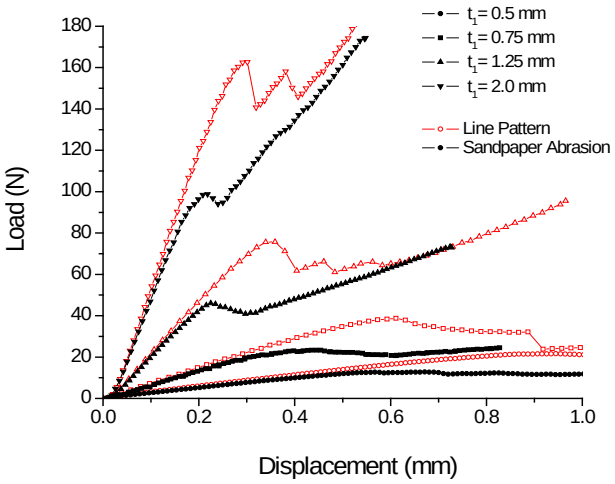

Fig. 8. Typical load-displacement curves of SLB tests with different mode-ratios.

The critical point at which the compliance has increased by 5% was interpreted as the on-set of crack propagation and used for the determination of critical load (P_c) as shown in Fig. 9. The initial compliance and pre-crack length of every tested specimen were used to determine the empirical $C = f(a)$ relationship (Fig. 10).

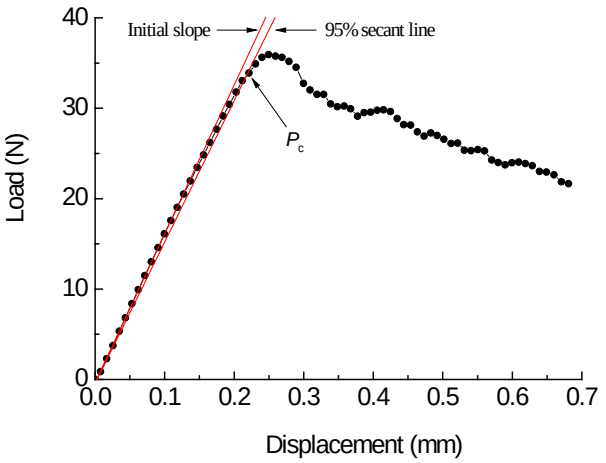

Fig. 9. Determination of initial compliance and P_c using a load-displacement curve.

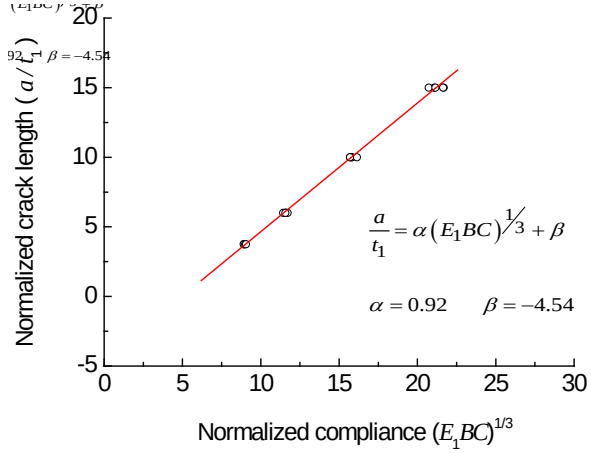

Fig. 10. Normalized compliance – crack length relationship (C=f(a)).

The critical load (P_c) of each SLB specimen was converted into interfacial toughness (G_c), and phase angle ($\psi = \tan^{-1}\sqrt{G_{II}/G_I}$) was used to quantify the mode-ratio. As shown in Fig. 11, micro-line patterned surface topography enhances bond strength in any loading mode, and the enhancement is prominent in opening-mode dominant loading.

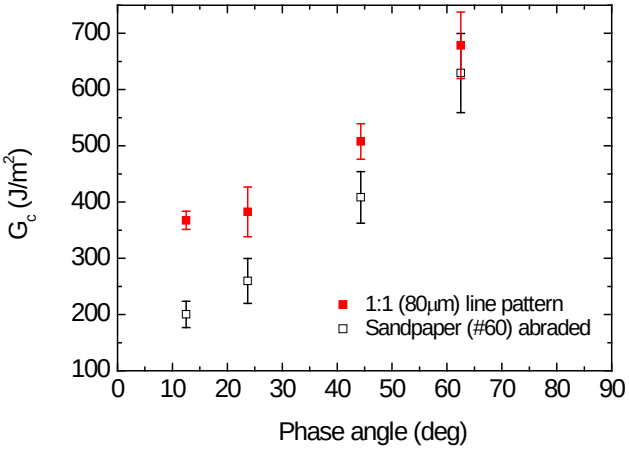

Fig. 11. Interfacial toughness (G_c) of composite/steel bonds according to various phase angle.

4.3 Crack propagation path observation

Figure 12 shows crack propagation paths observed using an optical microscope. In an opening-mode dominant loading condition, crack propagates along the polymer/metal interface with negligible adherend material damage. However, in a sliding-mode dominant loading condition, crack propagation induces considerable damage to polymer materials.

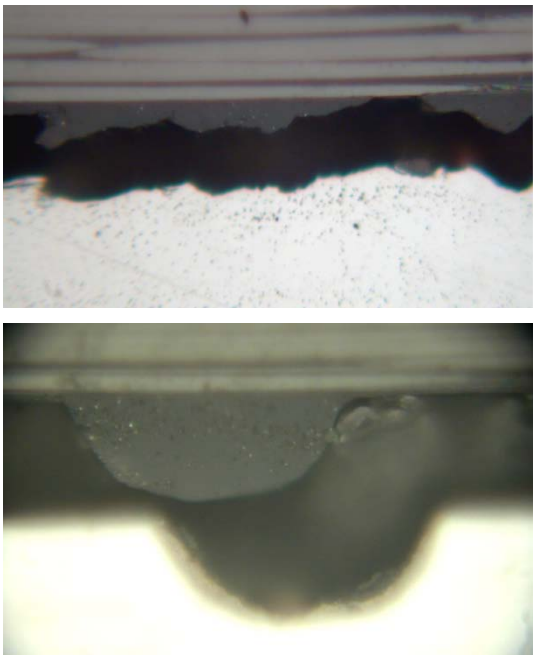

(a) Interfacial failure in opening-mode dominant loading (ψ=12°)

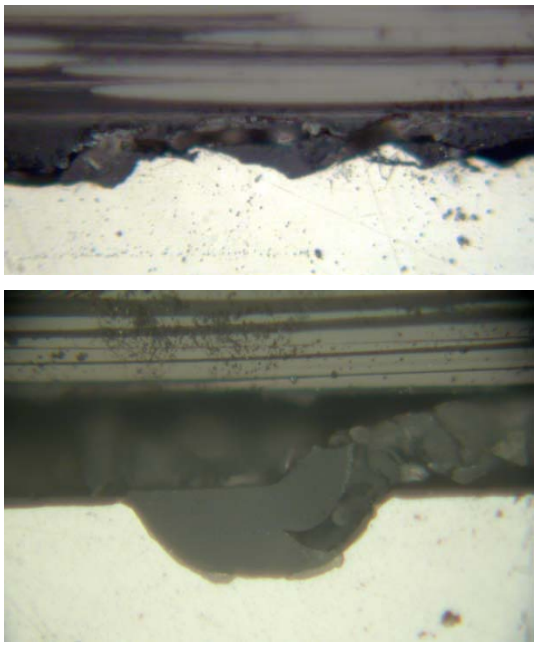

(b) Cohesive failure in sliding-mode dominant loading (ψ=64°)

Fig. 12. Crack propagation path deviation according to different loading modes.

The high interfacial toughness in sliding-mode dominant loading condition results from the increment of energy dissipation during crack propagation process. The higher interfacial toughness of micro-line patterned metal surface compared to sandpaper abraded surface caused from the increased damage zone in the polymer resin due to the reinforced mechanical interlocking (Fig. 12(b)). The micro-line pattern provided a microscopically screw-threaded structure at the interface, and it required more energy dissipation for crack growth.

5 Conclusions

The proposed micro-line patterned surface topography can provide higher enhancement of adhesion strength compared to conventional mechanically abraded surface morphology. The optimized surface topography for adhesion can be attained by maximizing the energy expense for crack growth, which eventually increases the resistance for crack propagation (G_c).

References

[1] A. Baker, S. Dutton and D. Kelly *"Composite Materials for Aircraft Structures"*. AIAA, 2004.

[2] R. Adams, *"Adhesive Bonding: Science, Technology and Applications"*. CRC Press, 2005.

[3] W. Brockmann, P.L. Geiß, J. Klingen, B. Schröder, *"Adhesive bonding: Materials, Applications and Technology"*. WILEY-VCH, 2009.

[4] P. Albrecht, A.H. Sahli, "Static strength of bolted and adhesively bonded joints for steel structures," *Adhesively bonded joints: testing, analysis and design, ASTM STP-981*, W.S. Johnson, Ed., Philadelphia, pp. 229-251, 1988.

[5] M.F. Fitzpatrick, J.S.G. Ling, J.F. Watts, "Failure mechanism of phosphated adhesively bonded hot-dipped galvanized steel: a small-area XPS study," *Surf. Interface Anal.* Vol. 29, pp. 131-138, 2000.

[6] P. Molitor, V. Barron, T. Young, "Surface treatment of titanium for adhesive bonding to polymer composites: a review," *Int. J. Adhes. Adhes.* Vol. 21, pp. 129-136, 2001.

[7] A. Baldan, "Review, Adhesively-bonded joints and repairs in metallic alloys, polymers and composite materials," *J. Mater. Sci.* Vol. 39, pp. 1-49, 2004.

[8] S.G. Prolongo, G. Rosario, A. Urena, "Study of the effect of substrate roughness on adhesive joints by SEM image analysis," *J. Adhesion Sci. Technol.* Vol. 20, pp. 457-470, 2006.

[9] J.R. Rice, "Elastic fracture mechanics concepts for interfacial cracks," *ASME J. appl. mech.* Vol. 55, pp. 98-103, 1988.

[10] B. Davidson and V. Sundararaman "A single leg bending test for interfacial fracture toughness determination". *Int. J. Fract.* Vol. 78, pp 193-210, 1996.

[11] ASTM D 3433 – Standard test method for fracture strength in cleavage of adhesives in bonded metal joints.

[12] ASTM D 5528 – Standard test method for mode I interlaminar fracture toughness of unidirectional fiber reinforced polymer matrix composites.

[13] ASTM D 6671 – Standard test method for mixed-mode interlaminar fracture toughness of unidirectional fiber reinforced polymer matrix composites.

[14] G.R. Irwin, J.A. Kies, "Critical energy release rate analysis of fracture strength," *Welding J.* Vol. 33, pp. 193-198, 1954.

[15] J.A. Nairn, "On the calculation of energy release rate for cracked laminates with residual stresses," *Int. J. Fract.* Vol. 139, pp. 267-293, 2006.